Vol 5 (1) (2024)

Measurement, Control, and Automation

Website: https:// mca-journal.org

ISSN 1859-0551

Parameter Optimization of Sliding Mode Controller for Tower Crane Using Particle Swarm Optimization Algorithm

Thi-Ly Tong[1], Minh-Trung Ho[2], Hoang-Hiep Dao[3], Vu-Khanh Pham[3], Minh-Duc Duong[3], Quy-Thinh Dao[3,]*

[1]*Faculty of Electrical Engineering, Hanoi University of Industry*
[2]*Military Environmental Chemistry Institute, Chemical Corps*
[3]*School of Electrical and Electronic Engineering, Hanoi University of Science and Technology*
**Corresponding author E-mail: thinh.daoquy@hust.edu.vn*

Abstract

Tower cranes find extensive application in the construction, ports, and industrial sectors for efficiently managing the transportation of heavy loads. However, operators face potential risks due to oscillations that occur during load movements. This not only diminishes operational efficiency but also poses significant hazards. Consequently, the control of tower cranes becomes a formidable challenge. To address this issue, various studies have been proposed, with particular attention given to the use of Sliding Mode Control (SMC). Vibrations caused by tower cranes have been mitigated by these studies. However, with SMC controllers for tower cranes, the problem of optimal parameter selection has not been adequately addressed by existing research. In this paper, a Particle Swarm Optimization (PSO) algorithm is used in conjunction with an SMC controller to determine the optimal parameter set for tower crane systems. A hierarchical sliding mode controller (HSMC) is utilized to control the position and minimize load oscillations. The PSO algorithm is applied to optimize the position settling time and angular deviation of the load. The SMC controller with the obtained optimal parameters achieves superior performance in tower crane systems, as demonstrated in simulations and experiments.

Keywords*: Hierarchical sliding mode controller, Particle swarm optimization, Sliding mode control, Tower crane.*

Symbols

Symbols	Units	Description
m_t, m_c	kg	Trolley mass and load mass
R	m	Trolley position
γ	Degree	Jib angle
α, β	Degree	Load angles on plane Oxz and Oyz
u_t	N	Trolley's control signal
u_r	Nm	Jib's control signal
l	m	Rope length
λ_1, λ_2, λ_3, λ_4, η_1, η_2, K_1, K_2		Controller parameter

Abbreviations

SMC	Sliding Mode Controllers
HSMC	Hierarchical Sliding Mode Controller
PSO	Particle Swarm Optimization

1. Introduction

Tower cranes are a vital component in the construction of tall buildings, massive structures, and complex projects. However, the crane operation is highly susceptible to the payload's oscillatory movements, which might put workers and equipment at risk. [1]. Typically, suppressing these movements calls for a more sophisticated control algorithm. A great variety of contributions to crane control can be found [2]. The proposed methods are mainly divided into two techniques including open-loop approaches and closed-loop approaches.

For open-loop control techniques, there are three widely used methods for tower crane systems which are command shaping [3], [4], filtering [5], [6], and command smoothing [7]–[9]. The advantage of these techniques is that they are simple to implement in practice, along with low cost. However, the impact of external disturbances such as wind, load changes, etc., on the system cannot be avoided. These noise effects cannot be eliminated using only open-loop control methods.

In the case of disturbances, closed-loop control techniques are more effective, the position of the load can be precisely controlled, and the system's swing angle can also be quickly suppressed. Regarding closed-loop control techniques, many controllers have been applied to tower crane systems such as linear control [10]–[14], predictive control [15], [16], adaptive control [17]–[20], fuzzy logic approaches [21]–[24], and sliding mode control [25]–[27], etc. Among these close-loop techniques, sliding mode control – SMC is a well-known method owing to its effectiveness, simplicity to implement in practice, stability, and robustness, even when the system encounters [28]. The efficiency of SMC for vibration suppression has been proven in [29]–[31]. However, up to now, only a few publications have mentioned the methods for selecting parameters for the controller as well as evaluating the

Received: 09 January 2024; Accepted: 20 February 2024.

effectiveness between different sets of parameters for the same system.

This article proposes an approach to designing a position and anti-vibration controller for tower cranes, based on the SMC method that integrates the following functions:

- A hierarchical structure for the sliding mode controller.
- Employing an optimization algorithm PSO for selecting SMC's parameter to reduce the system's setting time and lower the load's angle.

Because the tower crane is an under-actuated system, the hierarchical sliding controller was designed and utilized. In addition, the PSO algorithm will help to find parameter values to achieve the goal of optimizing setup time and reducing load swing angle deviation.

The rest of this paper is organized as follows: Section 2 introduces a dynamic model of a tower crane and details important components of this model; Section 3 presents the design of the SMC controller, developed for position control and vibration suppression of tower cranes. This is an important part, explaining in detail the SMC sliding control method and how to apply it to the tower crane system; Section 4 introduces the PSO optimization algorithm to adjust parameters in the controller. This section demonstrates how to apply the PSO algorithm to find optimal parameters for the SMC controller; Section 5 presents simulation results on Matlab/Simulink and provides results from the experimental model. This is the part to evaluates the performance and effectiveness of the proposed method through simulation and experimental results; Finally, Section 6 is the conclusion, summarizing the results and emphasizing the contributions and limitations of the research, while also suggesting future development directions.

2. Tower Crane system dynamic

The physical model of the tower crane illustrated in Figure 1, includes two motions which are the translation motion of the trolley on the jib and the slewing motion of the jib around the tower. The cargo mass m_c is attached to the trolley through a cable system that is responsible for lifting and lowering loads. When a force and a torque are acted on the trolley and the jib, the load will vibrate due to fictitious force during movement. In this system, considering only the translation motion and the slewing motion, ignoring the mass of the rope and the elastic deformation of the tower, assuming that the load angles are small, and the length of the cable stays unchanged, Euler-Lagrange equations are used to obtain the dynamics of the tower crane.

The kinetic energy of the tower crane is calculated as:

$$K = \frac{1}{2} m_t \dot{x}_t^2 + \frac{1}{2} m_c \dot{x}_c^2 + \frac{1}{2} J \dot{\gamma}^2 \quad (1)$$

where:

$\dot{x}_t$ is the velocity of the trolley.

$\dot{x}_c$ là the velocity of the load.

$\dot{\gamma}$ is the angular velocity of the jib.

The potential energy of the tower crane is determined as:

$$P = -m_c g l \cos\beta \cos\alpha \quad (2)$$

From (1) and (2), the Lagrange function is established as:

$$L = K - P = \frac{1}{2} m_t \dot{x}_t^2 + \frac{1}{2} m_c \dot{x}_c^2 + \frac{1}{2} J \dot{\gamma}^2 + m_c g l \cos\beta \cos\alpha \quad (3)$$

Figure 1. Tower crane model.

Corresponding to each state variable, the dynamic equations are established [32]:

$$\begin{cases} \dfrac{d}{dt}\left(\dfrac{\partial L}{\partial \dot{R}}\right) - \dfrac{\partial L}{\partial R} = u_t \\ \dfrac{d}{dt}\left(\dfrac{\partial L}{\partial \dot{\gamma}}\right) - \dfrac{\partial L}{\partial \gamma} = u_r \\ \dfrac{d}{dt}\left(\dfrac{\partial L}{\partial \dot{\alpha}}\right) - \dfrac{\partial L}{\partial \alpha} = 0 \\ \dfrac{d}{dt}\left(\dfrac{\partial L}{\partial \dot{\beta}}\right) - \dfrac{\partial L}{\partial \beta} = 0 \end{cases} \quad (4)$$

Ignoring the small complicated non-linear components, trigonometric approximations are also used to simplify the calculations (4), the dynamics model of the tower crane is obtained:

$$\begin{cases} \ddot{R} + \dfrac{m_c}{m_t} g\alpha = \dfrac{u_t}{m_t} \\ (1 + \dfrac{m_t}{J} R^2)\ddot{\gamma} - \dfrac{m_c}{J} gR\alpha = \dfrac{u_r}{m_t} \\ l\ddot{\alpha} + g\alpha - \ddot{R} = 0 \\ l\ddot{\beta} + g\beta + R\ddot{\gamma} = 0 \end{cases} \quad (5)$$

The differential equations in (5) describe the variation of state variables, including the trolley position R, the rotation angle γ of the jib, and the swing angles α and β of the load. The state variables depend on the input variables, including the force u_t acts on the trolley, the torque u_r acts on the jib, and model parameters such as m_t, l, m_c, J, and g.

In practice, the movement of the trolley R and the jib γ are controlled independently by two motors with drivers allowing us to control the speed of the trolley and the jib separately, accurately, and eliminate the effect of external disturbances. Although equation (5) has four state variables, there are only two actuators, making the system an under-actuated system. We can see that the first and second equations in (5) interact with the swing angle state variable α. However, in this study, by using motor drivers with ideal current loops and speed loops, the influence of angle α on the first two equations can be eliminated. Besides, because the inner circuit which is used to drive the motors, is much faster than the outer speed circuit,

according to [33] we can simplify the first equation. and the second of (5) as follows:

$$\frac{R(s)}{U_t(s)} = \frac{F_1}{s(T_1 s + 1)} \tag{6}$$

Where, U(s) is the Laplace transformation of the voltage signal control the trolley $u_t(t)$, $R(s)$ is the Laplace transformation of the position of the trolley $r(t)$, $F_1$is a gain factor, and T_1 is the time constant of the system.
Inverse Laplace transform equation (6), we have:

$$\ddot{R} + \frac{1}{T_1}\dot{R} = \frac{F_1}{T_1}u_t \tag{7}$$

Similarly, the model that controls the rotation angle of the jib can be expressed as:

$$\ddot{\gamma} + \frac{1}{T_2}\dot{\gamma} = \frac{F_2}{T_2}u_r \tag{8}$$

The dynamic model of the tower crane can be rewritten as follows:

$$\ddot{R} + \frac{1}{T_1}\dot{R} = \frac{F_1}{T_1}u_t \tag{9}$$

$$\ddot{\gamma} + \frac{1}{T_2}\dot{\gamma} = \frac{F_2}{T_2}u_r \tag{10}$$

$$l\ddot{\alpha} + g\alpha - \ddot{R} = 0 \tag{11}$$

$$l\ddot{\beta} + g\beta + R\ddot{\gamma} = 0 \tag{12}$$

It should be noted here that we will design the position and angle control by including the motor transmission system, so the input control signal has been converted to voltage. In this study, we will use equations (9)-(12) to design a controller for the tower crane in the next section.

3. Controller design and control parameter optimization

3.1. Design of the Hierarchical Sliding Mode Controller

According to the dynamics model (9)-(12), the tower crane is an under-actuated system. The purpose of this paper is to design a controller that drives the trolley and the jib to the desired position and reduces the swing angles of the cargo to zero. A hierarchical sliding mode control approach is proposed to control the under-actuated system such as the tower crane with u_t, u_r are the control inputs and R, γ, α, β are the system state. Designing of the HSMC includes two steps:

- First, a first-order sliding surface is defined to attract all state trajectories.
- Then a control scheme is built to force all system states to their reference values on the sliding surface.

Set the system state R, γ, α, β as state variables as follow:

$$\begin{aligned} &x_1 = R;\ x_2 = \dot{x}_1;\ x_3 = \gamma;\ x_4 = \dot{x}_3; \\ &x_5 = \alpha; x_6 = \dot{x}_5; x_7 = \beta; x_8 = \dot{x}_7 \end{aligned} \tag{13}$$

Define the regulation error vectors as follows:

$$e_1 = x_1 - x_{1d};\ e_3 = x_3 - x_{3d};\ e_5 = x_5;\ e_7 = x_7 \tag{14}$$

Substituting (13) into equations (9)-(12) and presenting them in the state-space model, one can obtain the state-space model of the tower crane as follows:

$$\begin{aligned} &\dot{x}_1 = x_2; \quad \dot{x}_2 = \frac{F_1}{T_1}u_t - \frac{1}{T_1}x_2; \\ &\dot{x}_3 = x_4; \quad \dot{x}_4 = \frac{F_2}{T_2}u_r - \frac{1}{T_2}x_4; \\ &\dot{x}_5 = x_6; \quad \dot{x}_6 = \frac{\dot{x}_2}{l} - \frac{gx_5}{l}; \\ &\dot{x}_7 = x_8; \quad \dot{x}_8 = -x_1\frac{\dot{x}_4}{l} - \frac{gx_7}{l}; \end{aligned} \tag{15}$$

Define the sliding surface as:

$$S = \begin{bmatrix} S_1 & S_2 \end{bmatrix}^T \tag{16}$$

Where:

$$\begin{aligned} S_1 &= \dot{e}_1 + \lambda_1 e_1 + \eta_1 \dot{e}_5 + \lambda_3 e_5 \\ S_2 &= \dot{e}_3 + \lambda_2 e_3 + \eta_2 \dot{e}_7 + \lambda_4 e_7 \end{aligned} \tag{17}$$

Differentiating equation (16) with respect to time, we have:

$$\begin{cases} \dot{S} = \begin{bmatrix} \dot{S}_1 & \dot{S}_2 \end{bmatrix}^T \\ \dot{S}_1 = \ddot{e}_1 + \lambda_1 \dot{e}_1 + \eta_1 \ddot{e}_5 + \lambda_3 \dot{e}_5 \\ \dot{S}_2 = \ddot{e}_3 + \lambda_2 \dot{e}_3 + \eta_2 \ddot{e}_7 + \lambda_4 \dot{e}_7 \end{cases} \tag{18}$$

Next, we choose the constant rate reaching law for the system:

$$\begin{cases} \dot{S}_1 = -K_1 sign(S_1) \\ \dot{S}_2 = -K_2 sign(S_2) \end{cases} \tag{19}$$

Substituting equations (15)-(18) into equation (19), the control signal can be established as:

$$\begin{aligned} u_t = \frac{1}{F_1(\eta_1 + l)}[&T_1\eta_1 g x_5 + l x_2 + \eta_1 x_2 \\ &+ T_1 l(\ddot{x}_{1d} - \lambda_1(x_2 - \dot{x}_{1d}) - \lambda_3 x_6) - T_1 l K_1 \operatorname{sgn}(S_1)] \end{aligned} \tag{20}$$

$$\begin{aligned} u_r = \frac{1}{F_2 J(l - \eta_2 x_1)}[&l x_4 - \eta_2 x_1 x_4 + T_2\eta_2 g x_7 \\ &+ T_2 l(\ddot{x}_{3d} - \lambda_2(x_4 - \dot{x}_{3d}) - \lambda_4 x_8) - T_2 l K_2 \operatorname{sgn}(S_2)] \end{aligned} \tag{21}$$

To reduce the effect of the chattering phenomenon, we replace the Sign function with a saturation function as follows:

$$sat\left(\frac{s_i}{\varepsilon}\right) = \begin{cases} sign(s_i) \text{ khi } |s_i| > \varepsilon \\ \dfrac{s_i}{\varepsilon} \text{ khi } |s_i| \le \varepsilon \end{cases}; \tag{22}$$

3.2. Stability analysis

To ensure the stability of the system, as a first step, we choose the Lyapunov function $V = \frac{1}{2}S^T S \ge 0$. Where: $\dot{V} = -K_1|S_1| - K_2|S_2| \le 0$ with every $K_1 > 0$, $K_2 > 0$. This means the system can maintain sliding on the sliding surface S = 0. However, for each sliding surface, it is a combination of the error between the output value compared to the setpoint value and the swing angle of the cargo. Thus, this combination doesn't guarantee that all the controlled variables will converge to their references on the sliding manifold. Therefore,

we need to consider the system state on the sliding surface. Substituting S = 0 into equation (17), then into equation (15). Through these transformations, we obtain a space-state model represented as follows:

$$\dot{Y} = AY \tag{23}$$

where $Y = [Y_1 \quad Y_2 \quad Y_3 \quad Y_4 \quad Y_5 \quad Y_6]^T$ with $Y_1 = x_5 = \alpha$; $Y_2 = x_7 = \beta$; $Y_3 = x_6 = \dot{x}_5$; $Y_4 = x_8 = \dot{x}_7$; $Y_5 = x_1 - x_{1d}$; $Y_6 = x_3 - x_{3d}$.

$$A = \begin{bmatrix} A_1 & A_2 & A_3 & A_4 & A_5 & A_6 \end{bmatrix}$$

where

$$A_1 = \begin{bmatrix} 0 & 0 & \frac{\lambda_1\lambda_3 - g}{(\eta_1 + l)} & 0 & -\lambda_3 & 0 \end{bmatrix}^T$$

$$A_2 = \begin{bmatrix} 0 & 0 & 0 & -\frac{x_1\lambda_2\lambda_4 + g}{l - \eta_2 x_1} & 0 & -\lambda_4 \end{bmatrix}^T$$

$$A_3 = \begin{bmatrix} 1 & 0 & \frac{\lambda_1\eta_1 - \lambda_3}{(\eta_1 + l)} & 0 & -\eta_1 & 0 \end{bmatrix}^T$$

$$A_4 = \begin{bmatrix} 0 & 1 & 0 & -x_1\frac{\lambda_2\eta_2 - \lambda_4}{l - \eta_2 x_1} & 0 & -\eta_2 \end{bmatrix}^T$$

$$A_5 = \begin{bmatrix} 0 & 0 & \frac{\lambda_1^2}{(\eta_1 + l)} & 0 & -\lambda_1 & 0 \end{bmatrix}^T$$

$$A_6 = \begin{bmatrix} 0 & 0 & 0 & -x_1\frac{\lambda_2^2}{l - \eta_2 x_1} & 0 & -\lambda_2 \end{bmatrix}^T$$

To guarantee the stability of the system, the linearized state matrix **A** should be Hurwitz (i.e. its eigenvalues are located in the left half of the complex plane). After a series of calculations, the stability conditions are given as:

$$\begin{cases} \lambda_1 > 0 \\ \eta_1 > -l \\ \lambda_3 > \lambda_1\eta_1 \\ \lambda_2 > 0 \\ \eta_2 x_{1d} < l \\ \lambda_4 x_{1d} < \lambda_2\eta_2 x_{1d} \end{cases} \tag{24}$$

With the proposed HSMC controller (20)-(21), the performance quality of the tower crane not only depends on model parameters such as *l, and J*, but also on the parameters of the controller including λ_1, λ_2, λ_3, λ_4, η_1, η_2, K_1, K_2. In this paper, we propose the use of the PSO algorithm to find the optimal parameters for the HSMC controller, with the goal of optimizing the settling time and swing angle error of the load.

3.3. HSMC's parameter optimization

In this paper, the PSO algorithm is used to obtain 8 parameters $\lambda_1, \lambda_2, \lambda_3, \lambda_4, \eta_1, \eta_2, K_1, K_2$ of the HSMC controller base on fitness function. How this fitness function is defined depends on the optimization target of each problem. As mentioned before, the goal of this research is to reduce the settling time. Furthermore, this paper also aims to lower the load's angle when the trolley and jig reach their reference position. From those targets, the fitness function for the PSO algorithm in this study is chosen as follows:

$$J = T_{xl} + \mu E_r \tag{25}$$

where

- T_{xl} is the 2% setting time of the system.
- $E_R = \sum_{t=T_{xl}}^{\infty}(|\alpha(t)| + |\beta(t)|)$ is the sum of swing angles after the system has settled.
- μ: weighting factor between T and e. If μ >1, PSO will prioritize for optimizing oscillations suppression. Otherwise, with μ <1 PSO will put more effort into reducing the settling time. In this article, the value of μ is chosen as 0.1.

The PSO algorithm is population-based optimization, where "particles" represent potential solutions. Particles move in the search space and interact with each other to search for the best location. The best location will correspond to the smallest fitness function value J.

The optimization will be done by adjusting the controller's parameter. With each set of parameters, the system will have a different response. Those responses will be evaluated by the fitness function. After many iterations of adjusting parameters and evaluating the response, the optimal parameters, which have a minimum value of J, are obtained.

From the works above, the whole control system can be summarized as in Figure 2.

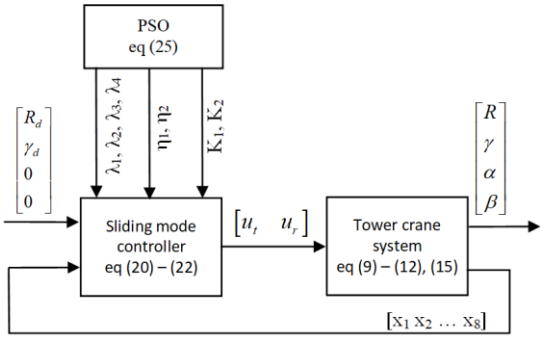

Figure 2. Tower crane control system diagram. Note that $x_1 = R, x_2 = \dot{x}_1, x_3 = \gamma, x_4 = \dot{x}_3, x_5 = \alpha, x_6 = \dot{x}_5, x_7 = \beta, x_8 = \dot{x}_7$.

4. Simulation and experimental results

4.1. Simulation and experimental setup

The parameter of the tower crane in this paper is: $T_1 = 0.01, T_2 = 0.08, F_1 = \frac{70\times2\times\pi\times0.016}{60}, F_2 = \frac{\left(\frac{10}{11}\right)\times2\pi}{60}, l = 0.59m,\ g = 9.81\frac{m}{s^2}$The starting positions of trolley and jib are R = 0 m and $\gamma = 0°$. The reference positions are $R = 0.3\ m, \gamma = 45°$. The boundary of controller parameters is detailed in (24). Control signal boundary is $\pm10V$ for u_t and $\pm10V$ for u_r.

In the next stage, PSO is started in Matlab/Simulink. First, a population of 50 particles is initialized. The maximum iteration is $K_{max} = 100$. With the PSO algorithm, the optimal parameter is obtained after K_{max} iterations.

This study is deployed on a tower crane model in the WSR laboratory of Hanoi University of Science and Technology. The tower crane model's structure is specified in Figures 3

and 4. The tower crane model has 2 moving axes driven by 2 servo transmission systems. Axis 1 is the rotation of the jib controlled by a servo motor accompanied by a high-ratio reduction gearbox. The transmission number is 1:11. The other axis is the forward motion of the trolley along the jib. The trolley is driven by a similar servo motor. Both motors used in the experiment are now in speed control mode. The entire system is controlled by the NI myRIO 1900 microcontroller, Table 1 describes the parameters of the servo motor. Labview software is used to program, control, and monitor the system. After obtaining the full parameters of the model and controller, the research was implemented on system simulation on Matlab/Simulink and then on the experimental model. Two scenarios are implemented in simulation and experiment to compare and evaluate the effectiveness of the parameter set that is determined by PSO:

- **Scenario 1:** The parameter of the SMC controller is selected manually.
- **Scenario 2**: Using the SMC controller parameters specified by the PSO algorithm.

Parameter sets of two scenarios are described in Table 2.

Table 1: Motor parameters

	Trolley's motor	Jib's motor
Rated output	200 W	200 W
Rated torque	1.27 N.m	1.27 N.m
Rated Speed	3000 rpm	3000 rpm
Inertia torque	$0.018 * 10^{-4}\ kg.m^2$	$0.018 * 10^{-4}\ kg.m^2$
Speed coefficient	$70\frac{rpm}{v}$	$10\frac{rpm}{v}$

Table 2: Controller parameters

SMC	SMC-PSO
$\lambda_1 = 1\ \ \lambda_2 = 0.9$	$\lambda_1 = 1.01\ \ \lambda_2 = 0.98$
$\lambda_3 = 1.1\ \ \lambda_4 = -1.5$	$\lambda_3 = 2.196\ \ \lambda_4 = -2.07$
$\eta_1 = 0.05$	$\eta_1 = 0.05$
$\eta_2 = -0.01$	$\eta_2 = -0.012$
$K_1 = 25\ \ K_2 = 70$	$K_1 = 35\ \ K_2 = 75$

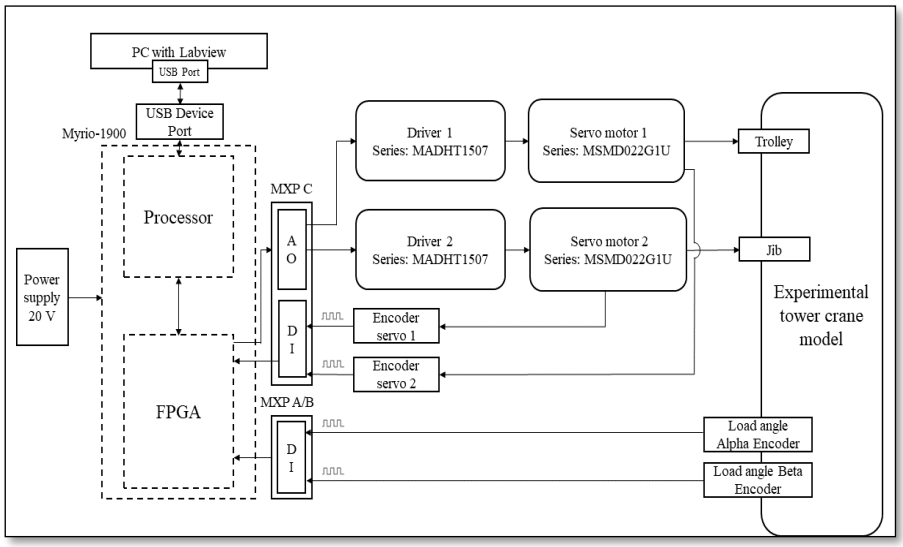

Figure 3. Experimental diagram.

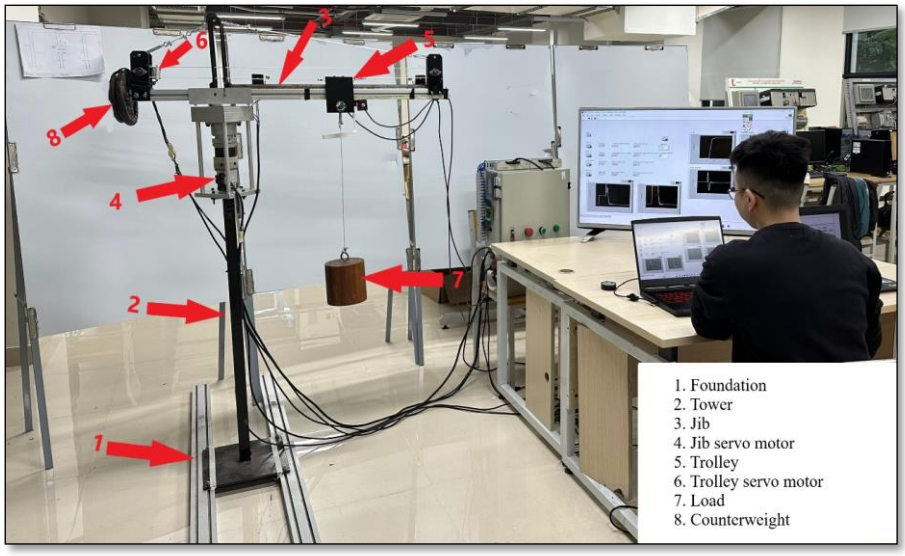

Figure 4. Experimental setup.

4.2. Simulation results

The results of the load angles α and β in Figure 5 show that with the use of the PSO-SMC controller, the settling time of the angles α and β are 2.5 seconds and 6.5 seconds, respectively. Meanwhile, when using the SMC controller without optimal parameters, the settling time of angles α and β is 7 seconds and 8.5 seconds. From these results, we can see the anti-vibration effectiveness of the PSO-SMC controller.

Figure 6 is the result of the position response R of the trolley and the rotation angle γ of the jib. The results show that when applying the PSO-SMC controller, the response time of rotation angle γ decreases from 4.2 seconds to 3.51 seconds. This result shows that the PSO algorithm has reduced the system setup time, as set out in section 4.1.

The voltage signals controlling the trolley u_t and the jib u_r are depicted in Figure 7, we can see that the PSO-SMC controller helps reduce the fluctuation of the control signal. This is achieved thanks to the rapid anti-vibration effect that the proposed controller provides.

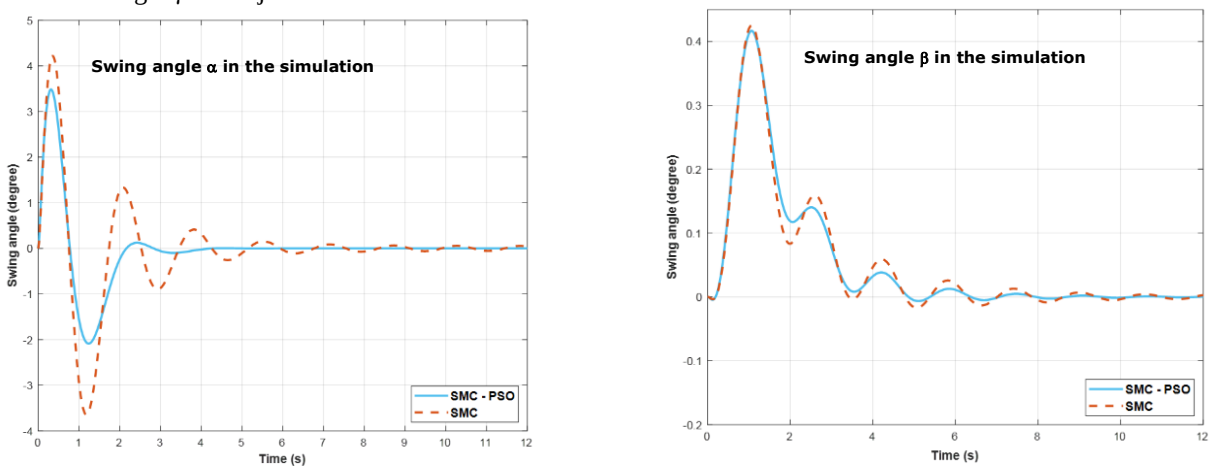

Figure 5. Load swing angle α and β in simulation.

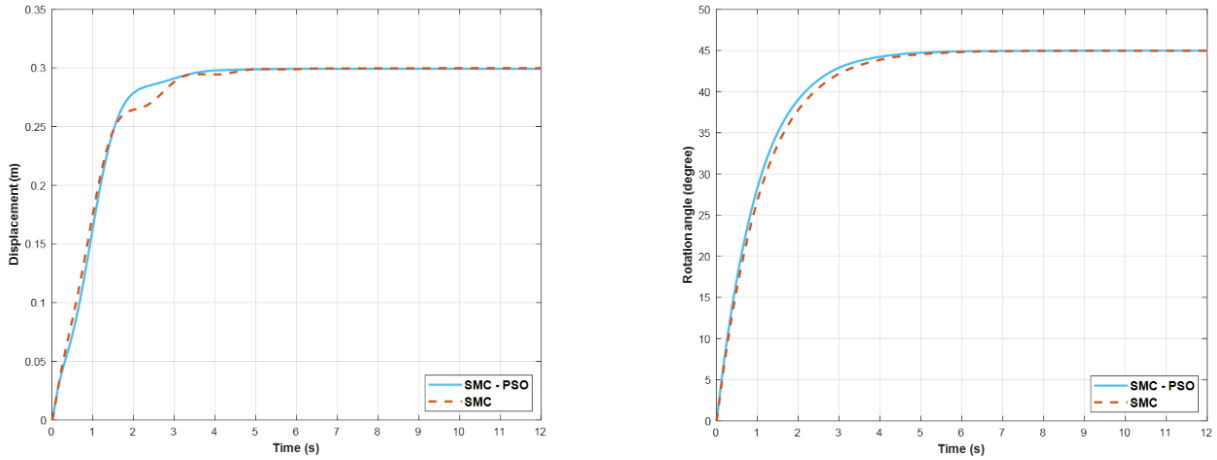

Figure 6. Trolley position in the jib and jib rotation angle in simulation.

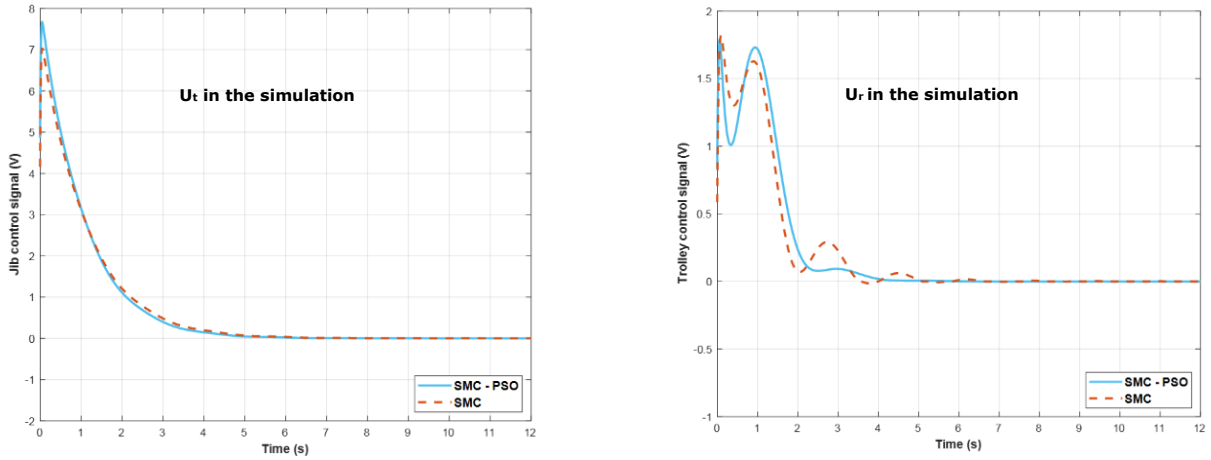

Figure 7. The control signal U_t and U_r in simulation

4.3. Experimental result

Experimental results Figure 8 verifies the anti-vibration effectiveness as mentioned in the simulation results above. When combining PSO with SMC, the oscillation angles α and β of the load are extinguished at the 5th second. Meanwhile, in the SMC controller with randomly selected parameters in scenario 1, the oscillation time of angles α and β is up to 11 seconds. Through this, we conclude that the PSO-SMC controller brings efficient oscillation suppression.

Figure 9 is the response of the trolley and jib when deployed on the experimental model. The jib settling time changes from 7.36 seconds to 6.27 seconds when applying the parameter set specified by PSO.

Figure 10 is the experimental result of the voltage signal controlling the trolley u_t and the jib u_r. Similar to the simulation results in Figure 6, when the oscillation phenomenon of the control signals u_r and u_t of the PSO-SMC controller is minimized.

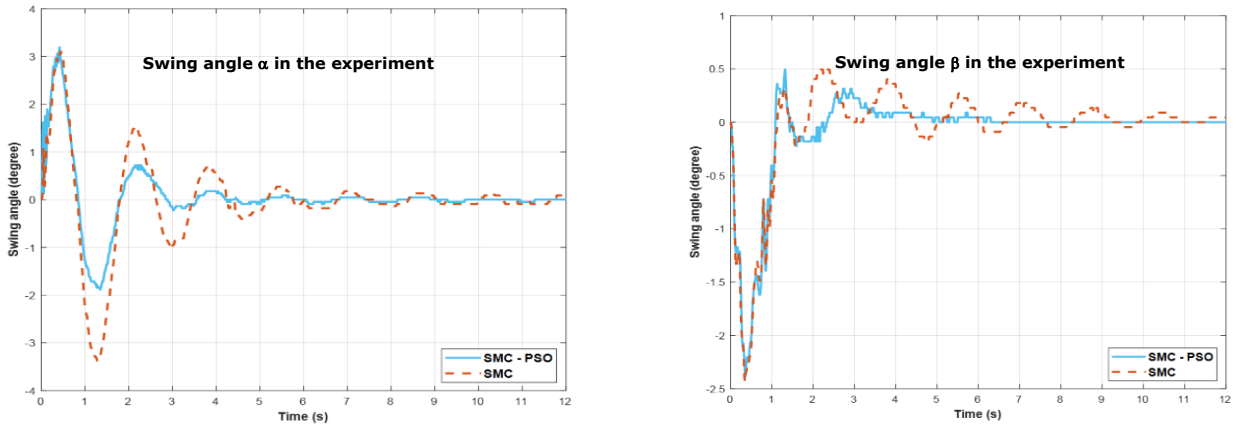

Figure 8. Load swing angle α and β in the experiment.

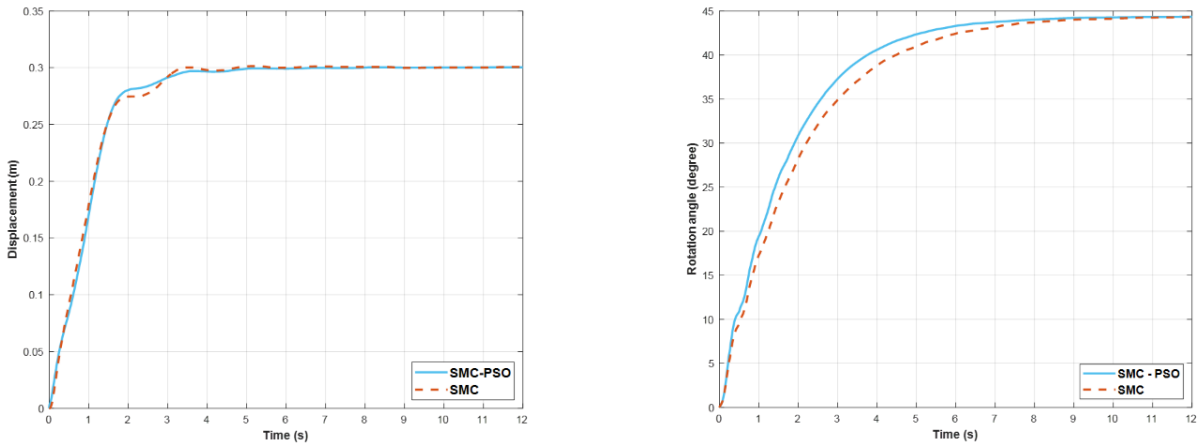

Figure 9. Trolley position in the jib and jib rotation angle in the experiment.

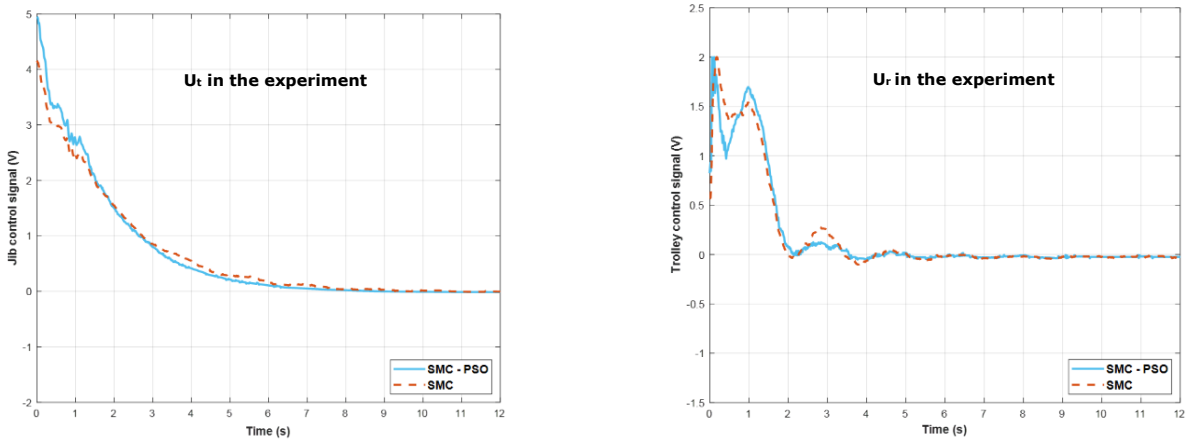

Figure 10. The control signal U_t and U_r in the experiment.

4.4. Evaluation of simulation and experimental results

From the results of simulation and experiment, we have a table of optimal results as shown in Table 3.

Table 3: Results comparison table.

		SMC	SMC-PSO
Simulation	System settling time	4.2s	3.51s
	Fitness function value J	4.34	3.53
Experiment	System settling time	7.36s	6.27s
	Fitness function value J	12.98	7.58

From Table 3, when using only the independent SMC controller, the settling time of the simulation system is 4.2 seconds, and the objective function value is 4.34. However, after integrating the PSO algorithm, this settling time is reduced to 3.51 seconds, and the objective function value is 3.53. In the experimental results, when using the PSO-SMC controller, the system settling time is only 6.27 seconds compared to 7.36 seconds when using the SMC controller. In addition, the objective function value is also reduced by 1.76 times.

Although there is a difference between the experimental and simulation results, both results show that the PSO-SMC controller provides higher anti-swinging performance and shorter settling time. This difference can be explained by the discrepancy between the real system and its mathematical model.

5. Conclusion

This article has presented an anti-vibration control method for tower cranes using the SMC sliding controller combined with the PSO optimization algorithm. Simulations and experiments have been implemented to demonstrate the correctness of this control method. After comparing the simulation and experimental results of the proposed controller with the SMC controller, some assessments are drawn including the PSO-SMC controller has a faster settling time (respectively 8.32% for simulation and 41.22% for experiment), along with the ability to suppress load vibrations faster as shown in Figure 4 and Figure 8. From these results, the combination between the PSO algorithm and SMC controller helps reduce system settling time, while improving anti-vibration efficiency.

However, the disadvantage of the SMC controller is that the system's control signals change too quickly. This phenomenon is called “Chattering”, which can cause high-frequency oscillations that adversely affect the system. Although after integrating the PSO algorithm, this phenomenon has been reduced thanks to the ability to quickly reduce vibration, the problem has not been completely resolved. Therefore, in the future, we will consider combining the PSO-SMC controller with the input signal shaping method. Finally, the above control method will also be considered and researched for implementation in tower crane systems with variable rope lengths.

References

[1] R.L. Neitzel, N.S.Seixas, and K.K. Ren, “A Review of Crane Safety in the Construction Industry: Applied Occupational and Environmental Hygiene: Vol 16, No 12.”

[2] L. Ramli, Z. Mohamed, A. M. Abdullahi, H. I. Jaafar, and I. M. Lazim, “Control strategies for crane systems: A comprehensive review,” *Mech. Syst. Signal Process.*, vol. 95, pp. 1–23, Oct. 2017, doi: 10.1016/j.ymssp.2017.03.015.

[3] Gordon G. Parker, Ben Petterson, Clark R. Dohrmann, and Rush D. Robinett III, “Vibration suppression of fixed-time jib crane maneuvers.”

[4] G. G. Parker, B. Petterson, C. Dohrmann and R. D. Robinett, “Command shaping for residual vibration free crane maneuvers,” Seattle, WA, USA: IEEE, 1995, pp. 934–938. doi: 10.1109/ACC.1995.529385.

[5] Q. Wu, X. Wang, L. Hua, and M. Xia, “Improved time optimal anti-swing control system based on low-pass filter for double pendulum crane system with distributed mass beam,” *Mech. Syst. Signal Process.*, vol. 151, p. 107444, Apr. 2021, doi: 10.1016/j.ymssp.2020.107444.

[6] D. Economou, C. Mavroidis and I. Antoniadis, “Comparison of filter types used for command preconditioning in vibration suppression applications,” Anchorage, AK, USA,: IEEE, 2022, pp. 2273–2278. doi: 10.1109/ACC.2002.1023979.

[7] J. Huang, Z. Liang, and Q. Zang, “Dynamics and swing control of double-pendulum bridge cranes with distributed-mass beams,” *Mech. Syst. Signal Process.*, vol. 54–55, pp. 357–366, Mar. 2015, doi: 10.1016/j.ymssp.2014.09.005.

[8] K. A. Alghanim, K. A. Alhazza, and Z. N. Masoud, “Discrete-time command profile for simultaneous travel and hoist maneuvers of overhead cranes,” *J. Sound Vib.*, vol. 345, pp. 47–57, Jun. 2015, doi: 10.1016/j.jsv.2015.01.042.

[9] R. Tang and J. Huang, “Control of bridge cranes with distributed-mass payloads under windy conditions,” *Mech. Syst. Signal Process.*, vol. 72–73, pp. 409–419, May 2016, doi: 10.1016/j.ymssp.2015.11.002.

[10] Shengzeng Zhang, Xiongxiong He, Haiyue Zhu, Xiaocong Li, and Xinggao Liu, “PID-like coupling control of underactuated overhead cranes with input constraints,” *ScienceDirect*, vol. 178, Oct. 2022, doi: 10.1016/j.ymssp.2022.109274.

[11] S. Chen, P. Xie, J. Liao, S. Wu, and Y. Su, “NMPC-PID control of secondary regulated active heave compensation system for offshore crane,” *Ocean Eng.*, vol. 287, p. 115902, Nov. 2023, doi: 10.1016/j.oceaneng.2023.115902.

[12] Hui Li, Yan-Ho Bui, Qiao Wang, Hong-Xiao Yang and Lin-Jun Wang, “Design of Anti-Swing PID Controller for Bridge Crane Based on PSO and SA Algorithm,” *Electronics*, vol. 11, no. 19, Sep. 2022, doi: 10.3390/electronics11193143.

[13] H. I. Jaafar, S. Y. S. Hussien, R. Ghazali and Z. Mohamed, “Optimal tuning of PID+PD controller by PFS for Gantry Crane System,” presented at the 2015 10th Asian Control Conference (ASCC), Kota Kinabalu, Malaysia, pp. 1–6. doi: 10.1109/ASCC.2015.7244695.

[14] F. Panuncio, W. Yu and X. Li, “Stable neural PID anti-swing control for an overhead crane,” presented at the 2013 IEEE International Symposium on Intelligent Control (ISIC), Hyderabad, India, 2013, pp. 53–58. doi: 10.1109/ISIC.2013.6658616.

[15] T. Baris̆a and M. Bartulovic, “Nonlinear Predictive Control of a Tower Crane using Reference Shaping Approach,” *Th Int. Power Electron. Motion Control Conf. Expo.*, 2014.

[16] P. Schubert and D. Abel, “Flatness-based Model Predictive Payload Control for Offshore Cranes,” in *2023 European Control Conference (ECC)*, Jun. 2023, pp. 1–8. doi: 10.23919/ECC57647.2023.10178159.

[17] N. Sun, Y. Fang, and H. Chen, “Adaptive antiswing control for cranes in the presence of rail length constraints and uncertainties,” *Nonlinear Dyn.*, vol. 81, Jul. 2015, doi: 10.1007/s11071-015-1971-y.

[18] J. Huang, W. Wang and J. Zhou, “Adaptive Control Design for Underactuated Cranes With Guaranteed Transient Performance: Theoretical Design and Experimental Verification,” vol. 69, no. 3, pp. 2822–2832, Mar. 2022, doi: 10.1109/TIE.2021.3065835.

[19] Menghua Zhang, Xin Ma, Xuewen Rong, Xincheng Tian, and Yibin Li, “Adaptive tracking control for double-pendulum overhead cranes subject to tracking error limitation, parametric uncertainties and external disturbances,” *Mech. Syst. Signal Process.*, vol. 76–77, pp. 15–32, 2016, doi: 10.1016/j.ymssp.2016.02.013.

[20] L. Yang and H. Ouyang, “Precision-positioning adaptive controller for swing elimination in three-dimensional overhead cranes with distributed mass beams,” *ISA Trans.*, vol. 127, pp. 449–460, Aug. 2022, doi: 10.1016/j.isatra.2021.08.035.

[21] T. Popadic, F. Kolonic, and A. Poljugan, “A fuzzy control scheme for the gantry crane position and load swing control,” vol. 3, Jan. 2006.

[22] L. Ramli, I. M. Lazim, H. I. Jaafar, and Z. Mohamed, “Modelling and Fuzzy Logic Control of an Underactuated Tower Crane System,” *Appl. Model. Simul.*, vol. 4, no. 0, Art. no. 0, Jan. 2020.

[23] Ling Ma, Xuyang Lou, Wei Wu and Xin Huang, “Neural network-based boundary control of a gantry crane system subject to input deadzone and external disturbance | Nonlinear Dynamics,” Mar. 2022, doi: 10.1007/s11071-022-07356-z.

[24] Y. Qian, H. Zhang and D. Hu, “Finite-Time Neural Network-Based Hierarchical Sliding Mode Antiswing Control for Underactuated Dual Ship-Mounted Cranes With Unmatched Sea Wave Disturbances Suppression,” *IEEE Transactions on Neural Networks and Learning Systems*, doi: 10.1109/TNNLS.2023.3257508.

[25] Qihang Guo, Lin Chai and Huikang Liu, “Anti-swing sliding mode control of three-dimensional double pendulum overhead cranes based on extended state observer,” 2023, doi: 10.1007/s11071-022-07859-9.

[26] N. B. Almutairi and M. Zribi, “Sliding Mode Control of a Three-dimensional Overhead Crane,” *J. Vib. Control*, vol. 15, no. 11, pp. 1679–1730, Nov. 2009, doi: 10.1177/1077546309105095.

[27] Le Anh Tuan, Jae-Jun Kim, Soon-Geul Lee, Tae-Gyoon Lim, and Luong Cong Nho, “Second-Order Sliding Mode Control of a 3D Overhead Crane with Uncertain System Parameters,” *Int. J. Precis. Eng. Manuf.*, vol. 15, 2014, doi: 10.1007/s12541-014-0404-z.

[28] S. J. Gambhire, D. R. Kishore, P. S. Londhe, and S. N. Pawar, “Review of sliding mode based control techniques for control system applications,” *Int. J. Dyn. Control*, vol. 9, no. 1, pp. 363–378, Mar. 2021, doi: 10.1007/s40435-020-00638-7.

[29] N. B. Almutairi and M. Zribi, “Sliding Mode Control of a Three-dimensional Overhead Crane,” *J. Vib. Control*, vol. 15, no. 11, pp. 1679–1730, Nov. 2009, doi: 10.1177/1077546309105095.

[30] L. A. Tuan and S.-G. Lee, “Sliding mode controls of double-pendulum crane systems,” *J. Mech. Sci. Technol.*, vol. 27, no. 6, pp. 1863–1873, Jun. 2013, doi: 10.1007/s12206-013-0437-8.

[31] K.-K. Shyu, C.-L. Jen, and L.-J. Shang, “Design of sliding-mode controller for anti-swing control of overhead cranes,” in *31st Annual Conference of IEEE Industrial Electronics Society, 2005. IECON 2005.*, Nov. 2005, p. 6 pp.-. doi: 10.1109/IECON.2005.1568895.

[32] Hanafy M. Omar, “Control of Gantry and Tower Cranes,” Blacksburg, Virginia, Jan. 2003.

[33] M. Böck and A. Kugi, “Real-time Nonlinear Model Predictive Path-Following Control of a Laboratory Tower Crane,” *IEEE Trans. Control Syst. Technol.*, vol. 22, no. 4, pp. 1461–1473, Jul. 2014, doi: 10.1109/TCST.2013.2280464.